Analyst

PAPER

View Article Online
View Journal | View Issue

Cite this: *Analyst*, 2014, **139**, 5772

Tailoring recognition clefts from non-specific recognition matrices in mixed molecular arrays†

Nivarthi Ramesh and Archita Patnaik

Received 22nd June 2014
Accepted 9th September 2014

DOI: 10.1039/c4an01120a

www.rsc.org/analyst

Multi-component organic interfaces with molecular-level mixing were prepared by integrating benzoic acid appended thiophene amphiphile [4-(6-(thiophene-3-carbonyloxy)hexyloxy)benzoic acid] (T6BA) and (±)-α-lipoic acid onto the Au surface. On a flat surface with infinite radii of curvature, T6BA and (±)-α-lipoic acid, endowed with chemically distinct end-groups, provided sufficient length mismatch to gain conformational entropy leading to stripe-like patterns when the immiscible ligands co-adsorbed. Good quality multi-component organic interfaces and molecular islands could be fabricated *via* composition variation of the participating ligands. Host–guest chemistry between benzoic acids and β-cyclodextrin was used to confirm the molecular-level mixing. T6BA and (±)-α-lipoic acid, each being a non-specific recognition matrix for dopamine, could thus be organized into mixed molecular arrays having well defined cavities for guest inclusion. This mixed molecular array behaved as a 'recognition matrix' for dopamine (DA, 15 nm) in the presence of ascorbic acid (AA). The surface patterns described here on a flat surface should in principle be applicable to other geometrical structures like spheres and cylinders. Further, charge transfer through the T6BA self-assembled monolayers depended on the anion type present in the supporting electrolyte, monitored through cyclic voltammetry.

1. Introduction

Contemporary biosensor devices are constructed either by mimicking specific recognition systems such as immobilized proteins and antibodies,[1,2] or using non-specific sensing relying on adsorption and diffusion processes.[3] Irrespective of specificity or non-specificity, well-defined multi-component interfaces are imperative for effective sensing. Lipoic acid has often been chosen as a matrix material in both 'specific' sensing as well as 'non-specific' sensing. For example, proteins and enzymes were successfully anchored onto gold nanoparticle/quantum dots and 'Au' substrates through cyclic disulphide linkage of lipoic acid.[4–7] In most cases, multiple fabrication steps were mandatory for creating patterned surfaces. The complexity increased further with multiple amphiphiles involved in the pattern formation. The combination of multiple amphiphiles upon co-assembly could either lead to summation of properties of the individual molecules or could give a totally new functionality which the individual molecules/amphiphiles lacked.[8] To this end, the simplest way to create mixed monolayer surfaces was by using a co-adsorption method involving wetting of the suitable binding substrates into mixed monolayer solutions of the corresponding amphiphiles.[9,10] If the concerned amphiphiles were endowed with varied functional moieties, complexities in fabricating monolayers with desired composition arose due to the difference in the strengths of adsorption. Further, if the functional moieties were different, the co-adsorption process led to phase separation/segregation giving rise to molecular island[11,12] formation. Also, the size distribution of these molecular islands depended on the shape of the substrate: whether a flat surface or a spherical nanoparticle surface. On a flat surface,[13,15] the mixed molecular monolayered domains were reported to have a wide size distribution range contrasting that of a narrower size distribution on a nanoparticle surface. Coarse-grained molecular dynamics simulations of multi-component domains on flat and cylindrical surfaces revealed the interplay of conformational entropy and enthalpy of phase separation as a cause of striped-domain formation when longer amphiphiles stayed with shorter ones at the domain boundaries.[14] Quy Khac Ong *et al.* characterized these striped-domains on Au-nanoparticles using high-resolution scanning tunneling microscopy. They have used molecules with similar (11-mercapto-1-undecanol/4-mercapto-1-butanol) and dissimilar (1-octanethiol/mercaptopropionic acid) functional groups to arrive at these striped domains.[16]

In the present work, we used mixtures of benzoic acid appended thiophene based amphiphiles with lipoic acid as a mixed molecular system to arrive at the striped domains on a flat substrate. Despite using chemically distinct end-groups with different strengths of adsorption, we were able to arrive at

Department of Chemistry, Indian Institute of Technology Madras, Chennai 600 036, India. E-mail: archita59@yahoo.com; Fax: +91 2257 4202

† Electronic supplementary information (ESI) available: Synthesis of the T6BA ligand system. See DOI: 10.1039/c4an01120a

different patterns by varying the composition. These striped domains were characterized by high-resolution atomic force microscopy (AFM) and electrochemically by cyclic voltammetry. We further demonstrate the application of striped domains in the field of biosensors to sense dopamine, a neuro-transmitter. Before the actual dopamine sensing, the striped domains were shown to consist of alternate layers of T6BA and (±)-α-lipoic acid. Host–guest chemistry between benzoic acid and β-cyclodextrin was used to confirm the molecular-level mixing. Cyclodextrins form inclusion complexes with a wide variety of guest molecules owing to the presence of lipophilic interior cavities.[17–19] Chemically, a single β-cyclodextrin molecule comprises of 7 D-(+) glucopyranose residues attached by α-(1,4) glucosidic bonds and geometrically is represented as a toroid, exposing secondary hydroxyl groups at the larger opening and primary hydroxyls at the smaller opening. As a result of this spatial projection, the interior is considerably less hydrophilic and is able to host hydrophobic guests primarily through non-covalent interactions. The average diameter of this interior cavity was estimated to be 0.69 nm, while that of the larger opening to be 0.84 nm bigger, rendering it an overall shape of a truncated cone. Finally, the mixed molecular array is presented as a 'recognition matrix' for dopamine.

2. Experimental section

2.1 General methods

All the reagents used in the present report were of highest purity and purchased from Aldrich Chemicals, Inc. and were used as such. All the solvents used in this study were of HPLC grade. If the solvent was water, it was triply distilled with a resistivity of 18.2 mΩ cm at 25 °C. β-Cyclodextrin was procured from Avra Synthesis Pvt. Ltd. The molecule T6BA is synthesized (ESI, Scheme 1†), purified and characterized (Fig. S1–S6†) prior to further experiments.

2.2 Preparation of silicon substrates

The silicon (100) wafers were soaked in 3 : 1 H_2SO_4–H_2O_2 (30%) solution (**Caution**: highly corrosive!) and then rinsed extensively with triple distilled water and ethanol solution.

2.3 Preparation of gold electrodes

All the gold electrodes (2 mm in diameter) for electrochemical measurements were polished with 0.3 μm alpha alumina powder & 0.05 μm gamma alumina powder on a felt pad for at least 20 min, then rinsed several times with ethanol and triple-distilled water, and finally sonicated in triple-distilled water and absolute alcohol for 15 min, successively. The polished electrodes were further immersed in a 0.5 M H_2SO_4 solution and cleansed electrochemically by applying consecutive cycles of negative potentials between −0.4 V and −1.2 V until the obtained voltammograms no longer changed and a characteristic voltammogram of a clean Au electrode was obtained. The electrodes thus cleaned were stored in millipore water for further use.

2.4 Preparation of self-assembled monolayers (SAMs) by the co-adsorption method

All the SAMs were generated by exposing the freshly cleaned gold substrates to T6BA and (±)-α-lipoic acid simultaneously in the solution phase. The concentrations of (±)-α-lipoic acid (1 mM) to T6BA (2 mM) were varied to attain a final ratio of 1 : 2. Mixed SAMs of (±)-α-lipoic acid and T6BA were prepared by immersing the gold substrate in the respective solutions in methanol for at least 24 hours. After formation of the SAM, the substrates were rinsed several times with methanol and dried under N_2 purging.

2.5 Atomic force microscopy

Mixed self-assembled monolayers fabricated by the co-adsorption method as well as solvent cast films were analyzed using an atomic force microscope (XE-100, Park Systems, Korea) in noncontact and contact modes. A 5 μm XY scanner head was used for operating in both contact and non-contact modes. The cantilevers (SHOCONA-SS and ACTA, AppNano) were fitted with monolithic, single crystal silicon tips with radii of curvature <5 nm. Probes used in noncontact mode imaging had a 300 kHz resonance frequency with a spring constant of 40 N m^{-1}. Images around 5 μm × 5 μm size were acquired with a scan rate of 1 Hz whereas images under 500 nm × 500 nm area were scanned at a rate of 2 Hz to 4 Hz and were analyzed using XEI image analysis software. To compensate for the sample tilt, all the images were subjected to first order plane fitting. All the images reported were raw and no filtering was applied after the first order plane fitting.

2.6 Computational methods

Geometry optimization of the monomers was done using density functional calculations at the B3LYP/6-31+G(d,p) level of theory, as included in the Gaussian 09 set of programs. ONIOM (B3LYP/6-31G(d):AM1) hybrid calculations were performed on T6BA/β-cyclodextrin inclusion complexes. All the optimizations were carried out with tight convergence criteria without any symmetry constraints. Geometry optimizations were then followed by frequency calculations to calculate the vibration modes of the molecules and also to ensure the global minimum of the stationary points. All the TDDFT (time-dependent density functional theory) calculations were performed at the B3LYP/6-31G(d) level of theory. To take solvent effects into consideration while experimental transition energies were compared with calculated excitation energies and oscillator strengths, the IEFPCM (integral equation formalism polarizable continuum model) was applied. Energy calculations were done for the first 25 vertical excited states.

2.7 Electrochemical techniques

Electrochemical measurements based on cyclic voltammetry (CV) and differential pulse voltammetry (DPV) were carried out using a CHI-910B electrochemical workstation (CH Instruments, USA). Measurements were performed in a three-electrode cell with Au as the working electrode and Pt wire as the

counter electrode. All potentials were recorded with respect to the Ag/AgCl (1 M KCl) reference electrode and with 0.1 M KCl as the supporting electrolyte in which 0.1 mM aqueous solution of $K_4[Fe(CN)_6]$ or $K_3[Fe(CN)_6]$ acted as the electroactive species. The solution was purged with N_2 before each experiment.

3. Results and discussion

3.1 Solution phase aggregation of multicomponent amphiphiles

The molecule T6BA (Fig. 1a), synthesized towards fabricating multi-component organic interfaces, can be represented as a molecular string bearing dual anchor units. The thiophene end can bind onto the gold surface whereas the benzoic acid functionality could be chemisorbed onto metal/metal oxide surfaces, such as ITO (or Silicon, SiO_2), in accordance with Pearson's HSAB principle. Our previous work on amphiphilized benzoic acids indicated very low critical aggregation concentrations[20] owing to hydrogen bond induced aggregation. T6BA rapidly aggregated in chloroform. Scanning probe microscopy and scanning electron microscopy were carried out to investigate the assembled patterns. Typically, 1 mM solutions when deposited onto silicon (100) substrates either by solvent-casting or by incubating the substrates, yielded ribbon-like aggregates. The isolated ribbons were ~300 nm wide and had lengths of a few hundreds of microns (Fig. 1b and c). The self-assembly of T6BA in non-polar solvents was mainly driven by acid dimerization due to benzoic acid functionalities. The ribbon-like aggregation is in striking contrast to our previous observations in non-thiophene appended systems[20] where benzoic acids primarily gave rise to ill-defined aggregates/precipitates with no specific geometry. The increase in concentration resulted in the decrease of aspect ratios (Fig. 1d and e).

Achieving good quality multi-component organic interfaces requires controlling of this hydrogen bonding. As polar solvents do not favor hydrogen bonding, the self-assembly process was followed in these solvents by monitoring the absorption spectral changes. Benzoic acid is reported to show a red shift if it acts as a proton acceptor and a blue shift if it behaves as a proton donor when ethereal solvents are added. In cases where it acts simultaneously as both a proton donor and a proton acceptor, red and blue shifts could occur in cases of dimerization and in the presence of ethanol, respectively.[21] The experimental absorption spectra of T6BA in methanol and chloroform solution are presented in Fig. 2a and c. The absorption maximum is red-shifted by 15 nm in methanol as the concentration of T6BA is increased (Fig. 2a). In a strong dielectric solvent environment, self-association of T6BA will be minimized due to strong solute–solvent interactions, primarily comprising of dipole and hydrogen bonded interactions.[22,23] In aliphatic alcohols like methanol, monomers are stabilized by hydrogen bonding with the solvent. T6BA exists as a H-bonded dimer in chloroform solution. An infinitely dilute solution of T6BA in chloroform would contain unsolvated monomeric molecules of T6BA and unsolvated dimers with increasing concentrations of the ligand. In view of the alcohol-assisted monomeric state of T6BA in methanol, further experiments involving sensor fabrication were done in the same solvent

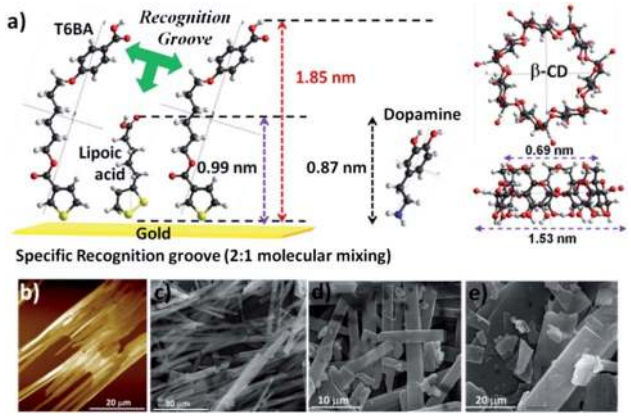

Fig. 1 (a) Geometry-optimized chemical structures under study. (b–e) depict recorded structural changes from topographic AFM imaging and scanning electron microscopy. (b) Non-contact mode AFM image of the self-assembled micro-ribbons of T6BA (1 mM) formed in chloroform solution. (c–e) SEM micrographs of T6BA at 1 mM, 3 mM and 5 mM, respectively.

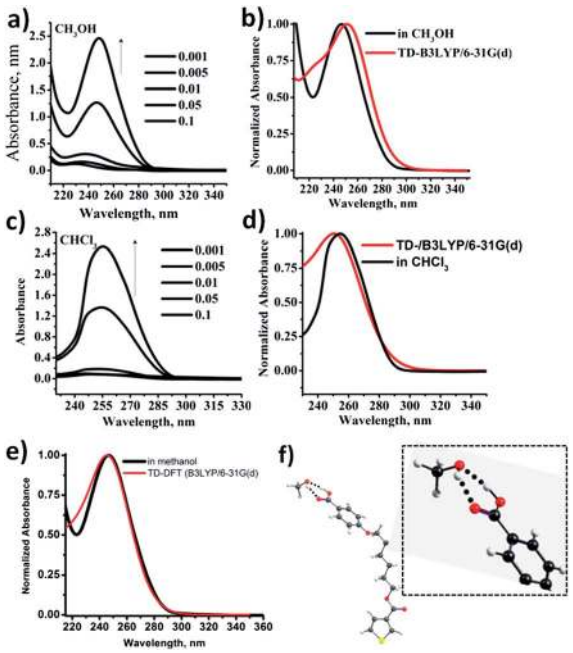

Fig. 2 The concentration (mM) dependent UV-visible absorption spectra of T6BA in (a) methanol and (c) chloroform. (b and d) Comparison of experimental *vs.* calculated absorption spectra of T6BA in methanol and chloroform, respectively. Experimental spectra were obtained in the respective solvents whereas calculated spectra were determined using TD-DFT (time dependent density functional theory) at the B3LYP/6-31G(d) level of theory with implicit solvation. (e) Comparison of experimental *vs.* calculated absorption spectra of T6BA in methanol where methanol is considered explicitly. (f) Methanol-assisted monomeric state computed at the B3LYP/6-31G(d) level of theory. All absorbances in the experimental/theoretical comparative plots were normalized to the absorbance maximum within the region shown.

medium. Computed electronic transitions using TD-DFT (time-dependent density functional theory) implemented in the Gaussian 09 set of programs matched with the experimental absorption spectrum. A comparison for T6BA in methanol is reported in Fig. 2b showing a single feature in the experimental spectrum. Further, good agreement between theory and experiment in terms of the band position is seen. The theoretical band is composed of two groups of transitions at 254.39 nm and 243.58 nm. The initial and final states of the band at 254.39 nm (oscillator strength, $f = 0.559$, $^1\pi$–π^*) are HOMO and LUMO+1, respectively. Both the states are localized on benzoic acid (Fig. S7†). Interestingly, the computed band at 243.58 nm is relatively weak with an oscillator strength of 0.023. HOMO−1 and LUMO are the initial and final states of the band at 243.58 nm ($^1\pi$–π^*) and are localized on the thiophene ring. Likewise, the computed band position for T6BA in chloroform is in agreement with the experimentally observed band feature. Moreover, computed spectra for monomeric T6BA underestimate the band position in chloroform (Fig. 2d) compared to overestimation in methanol (Fig. 2b). This indirectly evidences the existence of exclusive dimers in chloroform and hence, the underestimation when a monomer was computed. Experimental bathochromic shifts with increasing concentrations of T6BA in methanol (Fig. 2a) are solely due to the strong association of methanol with T6BA where the carbonyl group of the carboxylic acid is a proton acceptor. Additionally, the computed absorption spectra match well with experimental spectra (Fig. 2e) when the solvent is considered explicitly confirming the presence of the alcohol-assisted monomeric state (Fig. 2f) in methanol. The frontier molecular orbital isosurfaces derived through TDDFT for T6BA in methanol (IEFPCM model for solvation) are represented in Fig. S7.†

3.2 Multi-component anisotropic organic interfaces: fabrication of the sensor

As multi-component organic interfaces are the goal in building a sensing platform, self-assembly in methanol was studied at controlled compositions of T6BA and (±)-α-lipoic acid. Supported by absorption spectra and TD-DFT calculations, self-assembly in methanol was studied as monolayers can be grown easily. Previous efforts to generate multi-component organic interfaces relied predominantly on the co-adsorption of two or more ligands. These efforts were hampered by the tendency of the adsorbates to form single-component domains or "islands" on the surface. The possible modes of mixing of T6BA and (±)-α-lipoic acid on different flat surfaces are represented in Fig. 3. The mixing mode 3 represented in Fig. 3 is ideal for 'recognition and sensing' as recognition sites are developed in the process of chemisorption at the gold surface. High resolution atomic force microscopy in non-contact mode was used to probe the molecular level mixing of (±)-α-lipoic acid and T6BA.

Phase imaging was done additionally to bring subtle contrast to the force microscopic images. Ideal mixing, if not homogeneous, was seen in methanol at 1 : 2 composition of (±)-α-lipoic acid with T6BA on silicon (100) surfaces (Fig. 4a–c). The presence of stripe-like domains in the nanospheres is noticed in the phase image (Fig. 4d). Benzoic acid moieties are prone to bind onto the silicon surface rather than the thiophene functionality; the mode of molecular organization/the grooves in the striped

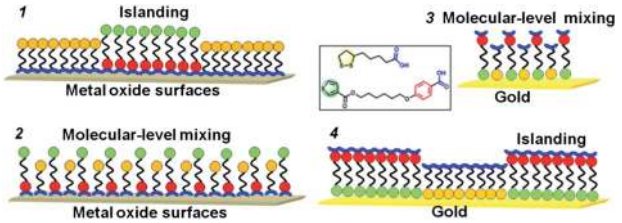

Fig. 3 Possible modes of 'mixing' of monolayers on the gold and metal oxide substrates. Functional groups bind to the substrate in accordance with Pearson's HSAB principle. Hard bases like carboxylates anchor to hard acids like metal oxides whereas soft bases like thiolates and thiophene bind onto soft acids like gold.

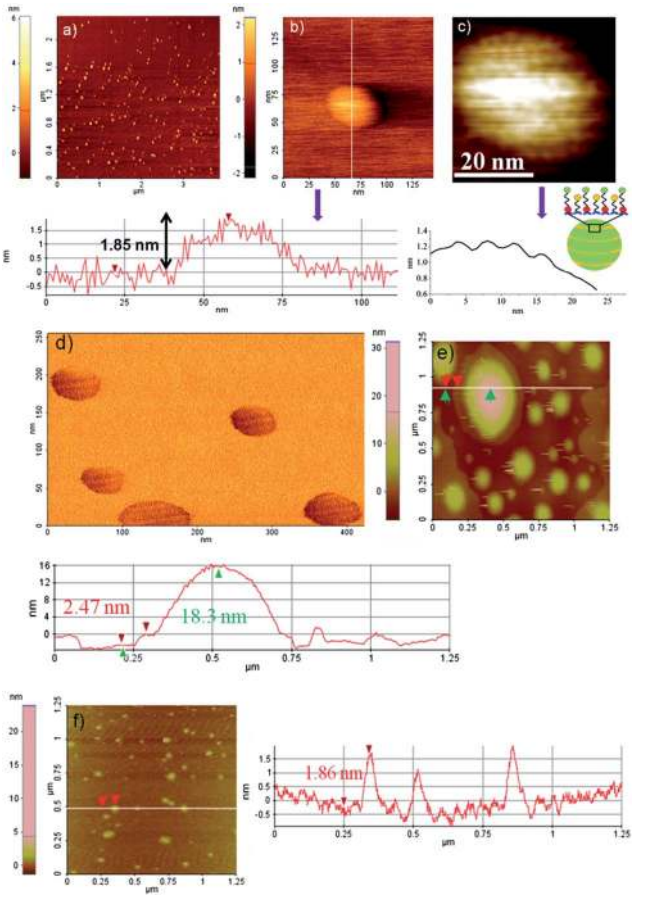

Fig. 4 (a–c) Topographic non-contact mode AFM images showing well-ordered multi-component domains of (±)-α-lipoic acid and T6BA mixed in 1 : 2 ratio on the Si (100) substrate with corresponding line profiles. The associated corrugated line profile on a single stripe-like domain indicates recognition sites present on the mixed SAM. Each recognition site is represented by a central (±)-α-lipoic acid surrounded by T6BA on either sides. (d) Phase image showing well-ordered and striped multi-component domains of (±)-α-lipoic acid and T6BA mixed in 1 : 2 ratio on the Si (100) substrate. (e) 1 : 1 and (f) 2 : 1 composition mixtures of (±)-α-lipoic acid and T6BA in methanol.

nanospheres are represented beside the line profile of Fig. 4c. The Glotzer group performed extensive atomistic and mesoscale simulations and STM imaging to explain the origin of experimentally observed stripe-like patterns formed by immiscible ligands (1-butanethiol and 1-hexanethiol), co-adsorbed on the surfaces of gold and silver nanoparticles.[24] Interestingly in the present experiments, (±)-α-lipoic acid and T6BA with spacers of C4 and C6 lengths showed striped patterns on a flat silicon surface. The length mismatch is significant enough to give a gain in conformational entropy and free volume by creating additional striped interfaces. The line profile on the striped particle in Fig. 4c indicates the clefts formed by an alternate arrangement of (±)-α-lipoic acid and T6BA. The line profile on a single striped nanosphere passing through the silicon surface indicates a height of 1.85 nm (Fig. 4b) which agrees with the DFT calculated height of T6BA. 1 : 1 and 2 : 1 compositions of (±)-α-lipoic acid–T6BA gave phase separated/segregated molecular islands (Fig. 4e) and randomly distributed nanospheres (Fig. 4f) ,respectively. The line profile across randomly distributed nanospheres indicates a height of 1.86 nm confirming the presence of T6BA monolayers in which (±)-α-lipoic acid is distributed in a random fashion. The line profile across the phase separated islands (Fig. 4e) indicates several nanometer heights owing to self-dimerization between T6BA molecules (or between (±)-α-lipoic acid molecules) as well as cross-dimerization between T6BA and (±)-α-lipoic acid. Additionally, experiments were carried out on ITO substrates where the benzoic acid moiety of T6BA and aliphatic carboxylate of (±)-α-lipoic acid chemisorb onto the ITO surface when co-adsorbed in 2 : 1 ratio. AFM topographic images of pristine T6BA SAMs in Fig. 5a and b showed ultrathin nanofibers of ~10 nm thickness and a height of a single monolayer. A 2 : 1 mixture (T6BA–lipoic acid) showed micro-phase separation (highlighted yellow coloured region in Fig. 5d) where nanofiber islands of T6BA arranged alternatively with the lipoic acid phase.

3.3 The striped T6BA monolayers and their β-CD inclusion complexes

The composition of T6BA and (±)-α-lipoic acid used in the formation of striped monolayers was employed for fabricating the mixed SAMs on a flat gold surface. Here, the thiophene part of T6BA and the disulphide moiety of lipoic acid were anchored onto the gold surface. The striped monolayer structure (now on the Au surface) from T6BA with alternating (±)-α-lipoic acid molecules was confirmed from the formed inclusion complexes of β-cyclodextrin with benzoic acid. Fig. 6a depicts a supramolecular approach to probe the molecular-level mixing through

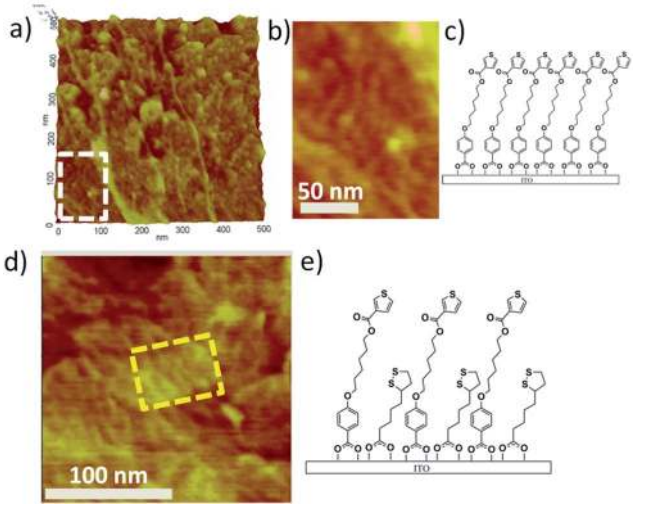

Fig. 5 Topographic non-contact mode AFM images of the self-assembled monolayers of (a) and (b) T6BA on the indium tin oxide (ITO) surface. (c) Schematic illustration of chemisorbed monolayers of pristine T6BA on the ITO surface. (d) Multicomponent organic interface of T6BA and (±)-α-lipoic acid (2 : 1) on the ITO surface along with the schematic illustration.

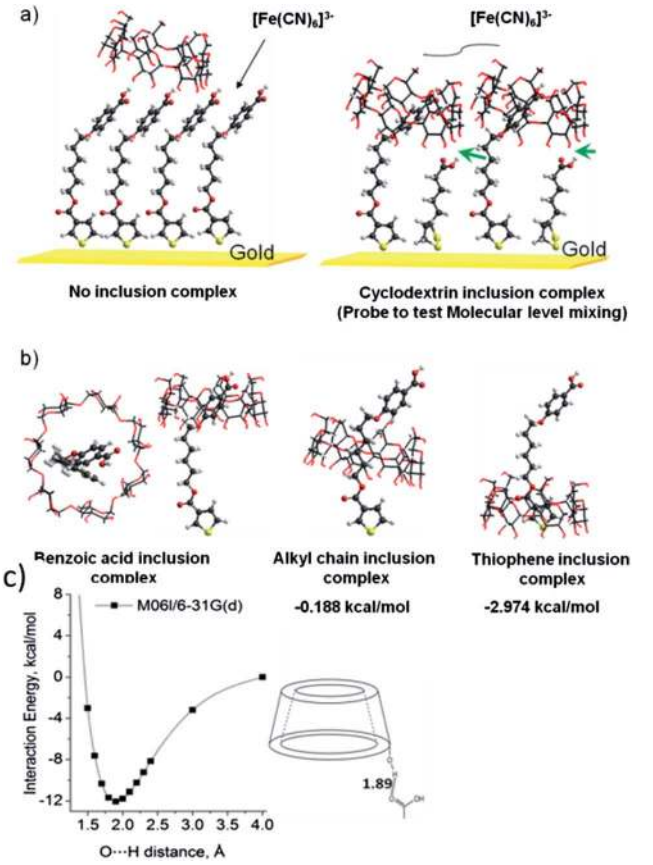

Fig. 6 (a) Single component SAM and multi-component SAM with islanding (not shown) show no inclusion complex formation. Internal negatively charged redox probe $[Fe(CN)_6]^{3-}$ will have little resistance due to the presence of T6BA SAM. Mixed SAM of (±)-α-lipoic acid with T6BA shows complex formation in which benzoic acid is hydrogen bonded with primary hydroxyl groups of cyclodextrin. The green arrows indicate possible hydrogen bond formation between aliphatic carboxylic acid of (±)-α-lipoic acid and secondary hydroxyl groups of β-CD. This additional hydrogen bond formation is expected to control the fast equilibrium between the monomer and host–guest complex. (b) Inclusion complexes of benzoic acid, alkyl chain and thiophene moieties with β-CD. (c) 1-D potential energy curve evaluated at the M06l/6-31G(d) level of theory by varying the H-bond distance between the β-CD and the aliphatic carboxylic acid of (±)-α-lipoic acid.

the use of β-cyclodextrin (β-CD), a class of truncated cone-shaped macrocyclic hosts with six glucopyranoside units, exposing primary (on the lower perimeter side) and secondary hydroxyl groups (on the higher perimeter side). β-CD can form stable 1 : 1 or 2 : 1 complexes with hydrophobic guests in water. T6BA having hydrophobic thiophene and comparatively less hydrophobic benzoic acid can form a 1 : 2 (two β-CDs) complex in the bulk and if anchored, can form a 1 : 1 complex. The formed inclusion complex could act as a molecular barricade by completely blocking electron transfer from the redox probe $[Fe(CN)_6]^{3-}$ to the gold working electrode, in the case of a voltammetry experiment (Fig. 6a). Benzoic acid forms inclusion complexes with both α- and β-CDs having association constants on the order of 550–750 M^{-1} and 48 M^{-1}, respectively.[25] This very low association constant of 48 M^{-1} with β-CD indicates a rapid equilibrium between the complex and the free molecules. This fast equilibrium can be controlled to an extent if the exterior hydroxyl groups can be indulged in hydrogen bonding (green arrows in Fig. 6a). The carboxylic acid group of the lipoic acid strongly binds with the secondary hydroxyl group of cyclodextrin by ~12 kcal mol^{-1}, thus slowing down the fast equilibrium process. The one-dimensional potential energy curve for this interaction is given in Fig. 6c.

In what concerns the inclusion compounds, several possible inclusion geometries were tested by full optimization calculations using the two-layer approximation of Morokuma *et al.*, as implemented in Gaussian 09 as ONIOM methodology.[26] It is observed from computed energies that the order of interaction of cyclodextrin with different functional groups (Fig. 6b) of T6BA is, benzoic acid (6.27 kcal mol^{-1}) > thiophene ester (2.97 kcal mol^{-1}) > alkyl chain (0.188 kcal mol^{-1}). The fact that AFM results in Fig. S8a,† where the stripe-like nanospheres were treated with β-CD solution in methanol, did not show any corrugated line profile as in the absence of β-CD suggests much more probability of complex formation if benzoic acid is present. This feature confirmed the presence of the thiophene/β-CD complex at the surface by filling the clefts, formed due to the alternate arrangement of T6BA and (±)-α-lipoic acid. Further, the absorption spectrum confirmed complex formation in the bulk phase with the T6BA/β-CD inclusion complex showing an absorption maximum, red shifted by 5 nm in comparison to an uncomplexed T6BA (Fig. S8b†).

3.4 Dopamine sensing in the mixed molecular arrays

Cyclic voltammograms were recorded for the mixed SAM on the Au electrode with 0.1 mM $Fe(CN)_6^{3-}$ as the redox probe and 0.1 M KCl as the supporting electrolyte. Cyclodextrin solution was injected into the electrochemical cell to make the cyclodextrin–T6BA complex and was kept for 6 h allowing sufficient time for the formation of the complex, following which cyclic voltammograms were recorded. The CV profiles in Fig. 7a confirm the formation of the T6BA/β-cyclodextrin complex due to which electron transfer across the surface has been blocked. Further, the complex formation could only be feasible for a specific orientation of lipoic acid and T6BA, as depicted in Fig. 6a.

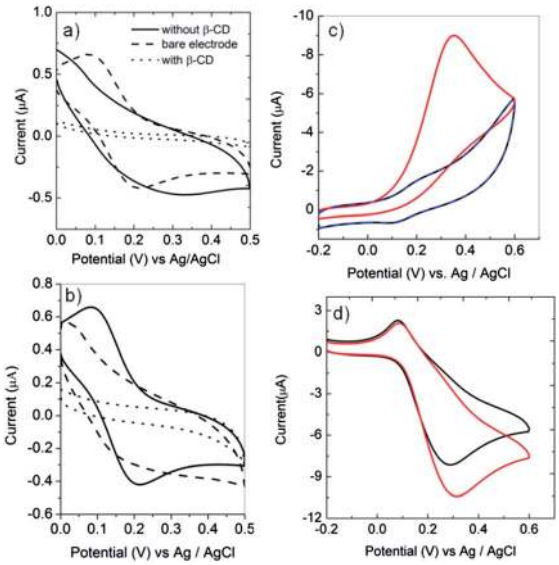

Fig. 7 (a) Cyclic voltammograms of $Fe(CN)_6^{3-/4-}$ in 0.1 M aqueous KCl at the bare Au electrode, the mixed SAM modified electrode without β-cyclodextrin and the mixed SAM modified electrode with β-cyclodextrin with 50 mV s^{-1} scan rate. (b) Cyclic voltammograms obtained from 0.1 mM $Fe(CN)_6^{3-}$ in 0.1 M KCl solution with the bare Au electrode at neutral pH (solid line), with the mixed SAM modified Au electrode at neutral pH (dashed line) and pH 9 (dotted line) at 50 mV s^{-1}. Cyclic voltammograms of 1 mM solution of (c) AA and (d) DA in 0.01 PBS buffer. The red line, blue line and the black line indicate the current responses for the bare Au electrode, the modified Au electrode in AA solution and the modified Au electrode in DA solution, respectively.

Fig. 7b shows the cyclic voltammograms obtained for the bare Au electrode and the mixed SAM modified Au electrode at neutral pH and at pH 9.0. Both the aliphatic and aromatic benzoic acids would be deprotonated at pH 9, giving rise to a negatively charged surface. It is apparent that electron transfer from $Fe(CN)_6^{3-}$ was nearly completely blocked at the modified Au electrode at pH 9. The CV results show that the response of the mixed SAM modified electrode is directly related to both solution pH and the probe's charge. This can be ascribed to the electrostatic environment at the film-solution surface. In PBS buffer solution, where the pH is 7.4, the surface carboxyl groups of lipoic acid (pK_a for aliphatic carboxyl groups ~4.76) and benzoic acid part of T6BA (pK_a for aromatic carboxyl groups ~4.2) are expected to dissociate. Thus, on the negatively charged film of the mixed SAM, the response of $Fe(CN)_6^{3-}$ was not observed. Electrostatic repulsion resists the access of $Fe(CN)_6^{3-}$ to the electrode surface. Further, it is found that in PBS buffer (pH 7.4), AA is negatively charged (Fig. A1 in the ESI†). In our experiments, after immobilization of lipoic acid and T6BA, the signal of AA was suppressed (Fig. 7c) to a great extent, which could be favorable for the detection of DA in a physiological environment. Moreover, DA has been found to be in a positively charged state up to pH 8.0 and thus it is expected to reach the electrode surface and undergo redox reaction (Fig. 7d). The results were in good agreement with a previous study.[27] The amino group of DA will be positively charged

($pK_b = 8.87$) at pH 7.4. This phenomenon of repelling negatively charged AA and attracting positively charged DA has been applied for the sensing of DA in the presence of high concentration of AA. Fig. 8a shows the cyclic voltammograms (CVs) of a mixed SAM modified Au electrode in PBS containing 0.2 μM DA and 0.2 μM AA. The CVs clearly show pairs of symmetric redox peaks that can be ascribed to the 'electron transfer–chemical reaction–electron transfer' (ECE) mechanism (Fig. A2 in the ESI†).

The anodic and cathodic peak currents, I_{pa} and I_{pc}, respectively were shown to increase linearly with the square root of the scan rate in the investigated range, from 20 to 200 mV s^{-1}, as shown in Fig. 8b. The linear relationship for the anodic peak current response is represented by $I_{pa} = 0.0574\nu^{1/2} - 0.185$, which suggests a diffusion-controlled oxidation of DA as the dominant mechanism. The selective determination of DA in the presence of ascorbic acid (AA) was investigated using differential pulse voltammetry (DPV). Fig. 9a shows the representative DPV curves of various DA concentrations in PBS solution (pH 7.0) in the presence of 1000 μM AA using the mixed SAM modified Au electrode. The peak currents assigned to the oxidation of DA (at 0.17 V *vs.* Ag/AgCl) show a linear response (Fig. 9b) with increasing DA concentration represented by, $I_p = -0.104C_{DA} - 0.63$, whereas no apparent DPV signal was observed for AA. The above experiment demonstrated selective detection of the mixed SAM modified electrode towards DA at DA/AA concentration ratios from 1 : 10 000 to 1 : 1000 ascribed mainly to electrostatic interactions. The sensitivity could be attributed to the combination of several positive attributes of the specific grooves created on the mixed molecular arrays (MMAs) at the Au surface, where DA could bind not only through electrostatic interactions, but also *via* hydrogen bond stabilization and π–π interactions (Fig. 10a). DFT calculations indicated the size of the formed groove to match with the size of the dopamine molecule, analogous to the lock and key mechanism (Fig. 10a). Additionally, the 1-D potential energy curve at the M062X/6-311++G(2d,2p) level of theory estimated the π–π interaction energy between dopamine and benzoic acid to be 11.6 kcal mol^{-1} (Fig. 10b). Further, the aliphatic carboxyl interacted with the positively charged dopamine with an estimated 86 kcal mol^{-1} through electrostatic and hydrogen bonding interactions, shown as H-bond assisted ion pair formation in Fig. 10c. This modified surface thus served as a specific sensor for DA. When AA was greater than DA, the change of AA at a constant concentration of DA did not cause any noticeable change of both peak current and peak potential of DA oxidation, indicating that the mixed SAM modified electrode was sensitive only to DA (Fig. 9d). On the other hand, when AA was less than DA at a constant concentration of DA, the variation of AA concentration had a significant influence on the peak current of DA oxidation (Fig. 9c). The results indicated that the peak current of DA oxidation increased with AA concentration and finally reached a plateau at an AA/DA ratio of 1. The above result shows the electro-catalysis of AA on DA oxidation,[27] in which the oxidized product of DA, dopamine-*o*-quinone, is chemically reduced by AA to DA again. When AA is less than DA (*i.e.*, AA concentration is lower than the oxidized form of DA), the limiting current apparently is controlled by the AA diffusion.

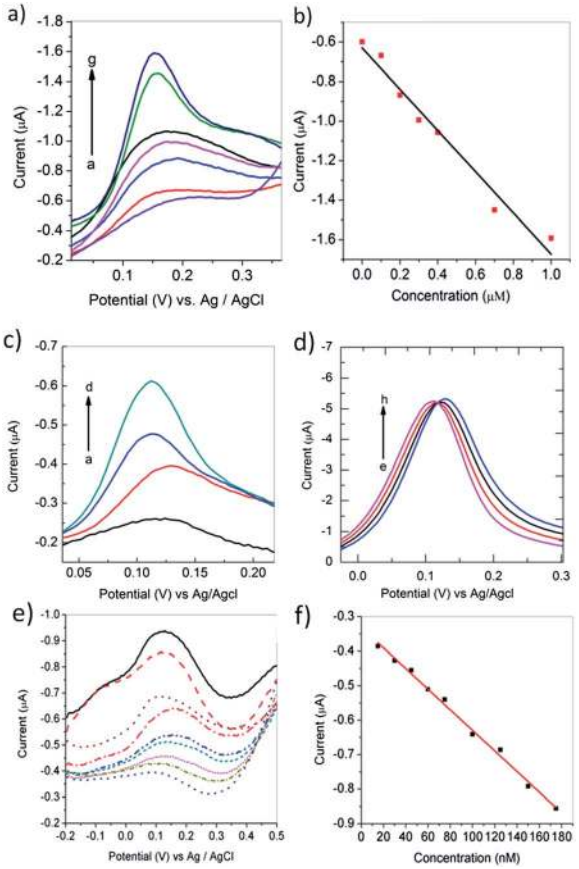

Fig. 9 (a) DPV for different concentrations of DA (a) 0, (b) 0.1, (c) 0.2, (d) 0.3, (e) 0.4, (f) 0.7 and (g) 1 μM in the presence of 1000 μM AA on the mixed SAM modified Au electrode in pH 7.4 PBS. (b) Calibration plots of peak current to the concentration of DA from DPV on the mixed SAM modified Au electrode. DPV of the mixed SAM modified Au electrode in PBS solutions with different AA/DA ratios. The DA concentration was 0.1 μM. (c) AA < DA: (a) 0.25 : 1; (b) 0.5 : 1; (c) 0.75 : 1; (d) 1 : 1. (d) AA > DA: (e) 2 : 1; (f) 3 : 1; (g) 4 : 1; (h) 5 : 1. (e) The DPVs at increasing concentrations of DA in 0.01 M PBS solution; DA concentration was varied as 15, 30, 45, 60, 75, 100, 125, 150 and 175 nM (from the bottom to the top respectively). (f) The calibration curve of DA obtained with the mixed SAM modified Au electrode in the presence of 100 μM AA and 5 μM UA.

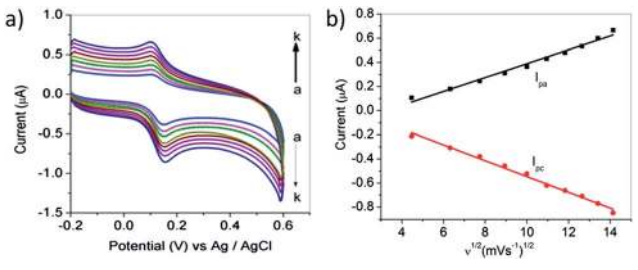

Fig. 8 (a) CV of the mixed SAM modified electrode in the solution of 0.2 μM DA and 0.2 μM AA solution (pH 7.4 PBS) at different scan rates (a–k): 20, 40, 60, 80, 100, 120, 140, 160, 180, and 200 mV s^{-1}; (b) calibration plots of peak currents to square root of scan rates were obtained from CV.

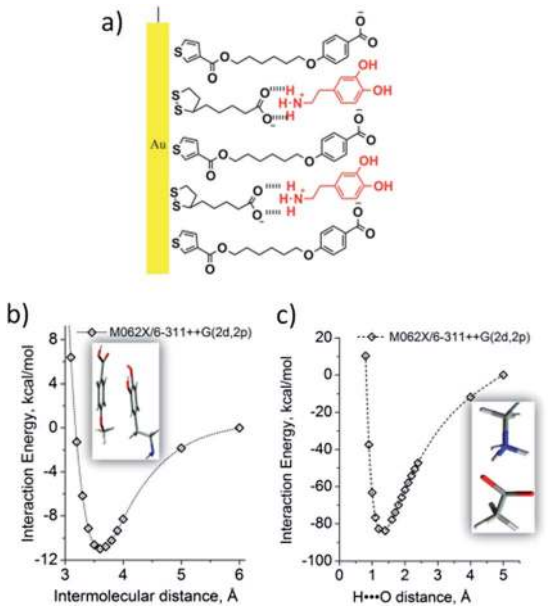

Fig. 10 (a) Mixed molecular array (MMA) on a gold surface with dopamine recognition sites. Binding mode of dopamine in the MMA recognition clefts. (b) 1-D potential energy curve for the estimation of the π−π stacking interaction between benzoic acid and dopamine. For simplicity and high accuracy in performing computations, the long alkyl chain of T6BA is mutated while dopamine is deprotonated. Calculations were performed at the M062X/6-311++G(2d,2p) level of theory. (c) 1-D potential energy curve of the dopamine interaction with carboxyl of lipoic acid in the recognition cleft performed at the M062X/6-311++G(2d,2p) level of theory. The figure on the right side illustrates the H-bond assisted ion-pair formation.

This explains the fact that the peak current increases linearly against the increase of AA when AA is less than DA. However, when AA is greater than DA, the oxidized form of DA is lower than AA concentration and the electrolytic current is then limited by DA. This is the reason why the electrocatalytic current reached a plateau at an AA/DA ratio of 1 as shown in Fig. 9d. Uric acid (UA) can also cause serious interference with the electrochemical detection of DA. Fig. 9e shows the DPV responses at various concentrations of DA at the modified Au electrode in the presence of 100 μM AA and 5 μM UA. Fig. 9f demonstrates that the DPV responses are linearly related to the DA concentration when very low concentrations of DA has been used in the presence of comparatively higher concentrations of AA and UA. In the DPV curve, the redox peak for UA is not observed which has been seen at around 0.35 V for the modified electrode reported by Wu *et al.*[28] This implies that the presence of AA and UA has negligible effects on the detection of DA, which demonstrates the excellent selectivity of this sensor.

3.5 Nanoseiving through T6BA self-assembled monolayers

We examined the integrity of pristine T6BA SAMs in terms of probable defects near the domain boundaries and whether they have any specific bearing on charge transport. The apparent electron transfer rate across the T6BA SAM modified Au (111) electrode was estimated from varied scan rates and their impact on the cathodic and the anodic peak potentials. We observed that as the scan rate increased, the reaction departed from the Nernstian behavior resulting in a quasi-reversible cyclic voltammogram with a larger ΔE_{peak} between $E_{p,a}$ and $E_{p,c}$ and an increased peak current. In an attempt to determine the electron transfer rate constant k, Laviron's approach,[29,30] valid for quasi reversible processes, was used. In Fig. 11, the cyclic voltammograms for the T6BA SAM modified Au electrodes in different electrolytes are shown. The calculated electron transfer rate constants for the T6BA SAM modified gold electrode were found to be 1.25×10^{-3}, 1.29×10^{-3}, 0.31×10^{-3} and 0.16×10^{-3} cm s^{-1} in KCl, K_2SO_4, KNO_3 and $KClO_4$, respectively. From the voltammograms as well as the heterogeneous rate constant values we could see that the electrode kinetics slowed significantly, as indicated by the reduced peak currents. These results imply anion dependence of charge transfer across the T6BA SAMs. 1-Adamantanethiol monolayers on gold were previously reported to show anion-dependent charge transfer.[31] In their report, the authors stated that nanopores formed by defects in the SAM or in the interstitial space between 1-adamantanethiol monolayers had acted as nanoscopic sieves (Fig. 11e) that selectively passed anions depending on the size and hydrophilic

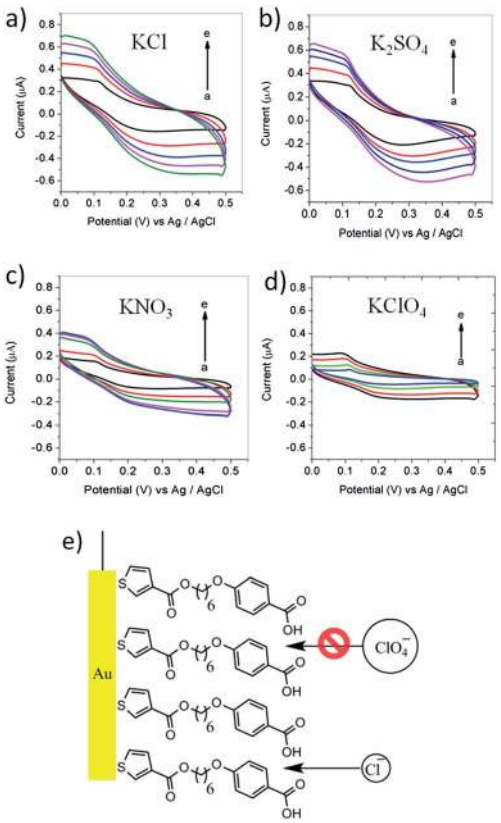

Fig. 11 CVs for the redox reaction of 0.1 mM $Fe(CN)_6^{3-}$ with different supporting electrolytes: (a) 0.1 M KCl, (b) 0.1 M K_2SO_4, (c) 0.1 M KNO_3 and (d) 0.1 M $KClO_4$, on the T6BA SAM modified gold electrode at various scan rates: (a) 20 mV s^{-1}, (b) 40 mV s^{-1}, (c) 60 mV s^{-1}, (d) 80 mV s^{-1} and (e) 100 mV s^{-1}. (e) Diffusing anions toward the T6BA SAM modified gold electrode. The arrows indicate anion flux during electrolysis.

properties. In addition, the presence of SAM perturbed the anion diffusion flux by modifying the double layer structure of the electrode or changed the other mass transport characteristics. In the present work, it is interesting that T6BA SAM exhibited the nanoseiving behavior towards anions, but additional experiments were required to ascertain whether this specific behavior had roots in the defective SAM formation.

4. Conclusions

In a unique attempt, the principle of simple co-adsorption of immiscible ligands onto a gold surface was adopted in fabricating a specific biosensor based on non-specific matrices containing aromatic and aliphatic carboxylic acids. Additionally, fabrication of the biosensor required a specific composition ratio of the multiple ligands. The molecular coordinates, such as the lengths of the monolayers in the mixed SAM, were ideally suited to hold dopamine, the neurotransmitter inside the recognition groove. The developed sensor could be used successfully to sense dopamine at low concentration levels even in the presence of interfering molecules like ascorbic acid and uric acid. The designed and fabricated self-assembled monolayers of T6BA on the Au electrode were well ordered and were shown to have nano-sieving functionalities for anions.

Acknowledgements

The authors thank the Department of Science and Technology, New Delhi, India (Grant no. SR/S2 CMP-57/2006). NR acknowledges the Senior Research Fellowship from IIT Madras. The Computer Centre, IIT Madras is gratefully acknowledged for providing the computational facilities.

Notes and references

1 K. E. Nelson, L. Gamble, L. S. Jung, M. S. Boeckl, E. Naeemi, S. L. Golledge, T. Sasaki, D. G. Castner, C. T. Campbell and P. S. Stayton, *Langmuir*, 2001, **17**, 2807.
2 J. Spinke, M. Liley, F. J. Schmitt, H. J. Guder, L. Angermaier and W. Knoll, *J. Chem. Phys.*, 1993, **99**, 7012.
3 K. Motesharei and M. R. Ghadiri, *J. Am. Chem. Soc.*, 1997, **119**, 11306.
4 J. M. Abad, S. F. L. Mertens, M. Pita, V. M. Fernández and D. J. Schiffrin, *J. Am. Chem. Soc.*, 2005, **127**, 5689.
5 M. Wipf, R. L. Stoop, A. Tarasov, K. Bedner, W. Fu, I. A. Wright, C. J. Martin, E. C. Constable, M. Calame and C. Schönenberger, *ACS Nano*, 2013, **7**, 5978.
6 J.-Y. Park, Y.-S. Lee, B. H. Kim and S.-M. Park, *Anal. Chem.*, 2008, **80**, 4986.
7 N. Zhan, G. Palui, M. Safi, X. Ji and H. Mattoussi, *J. Am. Chem. Soc.*, 2013, **135**, 13786.
8 Y. Liu, Y. Li, J. He, K. J. Duelge, Z. Lu and Z. Nie, *J. Am. Chem. Soc.*, 2014, **136**, 2602.
9 C. D. Bain and G. M. Whitesides, *J. Am. Chem. Soc.*, 1988, **110**, 3665.
10 C. D. Bain and G. M. Whitesides, *J. Am. Chem. Soc.*, 1988, **110**, 6560.
11 N. J. Brewer and G. J. Leggett, *Langmuir*, 2004, **20**, 4109.
12 S. J. Stranick, A. N. Parikh, Y. T. Tao, D. L. Allara and P. S. Weiss, *J. Phys. Chem.*, 1994, **98**, 7636.
13 R. P. Carney, G. A. DeVries, C. Dubois, H. Kim, J. Y. Kim, C. Singh, P. K. Ghorai, J. B. Tracy, R. L. Stiles, R. W. Murray, S. C. Glotzer and F. Stellacci, *J. Am. Chem. Soc.*, 2007, **130**, 798.
14 C. Singh, P. K. Ghorai, M. A. Horsch, A. M. Jackson, R. G. Larson, F. Stellacci and S. C. Glotzer, *Phys. Rev. Lett.*, 2007, **99**, 226106.
15 W. A. Hayes, H. Kim, X. Yue, S. S. Perry and C. Shannon, *Langmuir*, 1997, **13**, 2511.
16 Q. K. Ong, J. Reguera, P. J. Silva, M. Moglianetti, K. Harkness, M. Longobardi, K. S. Mali, C. Renner, S. De Feyter and F. Stellacci, *ACS Nano*, 2013, **7**, 8529.
17 J. H. Park, S. Hwang and J. Kwak, *ACS Nano*, 2010, **4**, 3949.
18 A. Harada, *Acc. Chem. Res.*, 2001, **34**, 456.
19 V. Bernat, C. Ringard-Lefebvre, G. Le Bas, B. Perly, F. Djedaïni-Pilard and S. Lesieur, *Langmuir*, 2008, **24**, 3140.
20 N. Ramesh, N. K. Sarangi and A. Patnaik, *J. Phys. Chem. B*, 2013, **117**, 5345.
21 M. Ito, H. Tsukioka and S. Imanishi, *J. Am. Chem. Soc.*, 1960, **82**, 1559.
22 H. E. Ungnade and R. W. Lamb, *J. Am. Chem. Soc.*, 1952, **74**, 3789.
23 H. H. Pham, C. D. Taylor and N. J. Henson, *J. Phys. Chem. B*, 2012, **117**, 868.
24 C. Singh, P. K. Ghorai, M. A. Horsch, A. M. Jackson, R. G. Larson, F. Stellacci and S. C. Glotzer, *Phys. Rev. Lett.*, 2007, **99**, 226106.
25 D. Salvatierra, C. Jaime, A. Virgili and F. Sánchez-Ferrando, *J. Org. Chem.*, 1996, **61**, 9578.
26 S. Dapprich, I. Komáromi, K. S. Byun, K. Morokuma and M. J. Frisch, *J. Mol. Struct.: THEOCHEM*, 1999, **462**, 1–21.
27 Y. Xiao, C. Guo, C. M. Li, Y. Li, J. Zhang, R. Xue and S. Zhang, *Anal. Biochem.*, 2007, **371**, 229.
28 T. Qian, S. Wu and J. Shen, *Chem. Commun.*, 2013, **49**, 4610.
29 E. Laviron, *J. Electroanal. Chem. Interfacial Electrochem.*, 1979, **100**, 263.
30 E. Laviron, *J. Electroanal. Chem. Interfacial Electrochem.*, 1979, **101**, 19.
31 J. H. Park, S. Hwang and J. Kwak, *ACS Nano*, 2010, **4**, 3949.

